Structure and the role of filling rate on model dsDNA packed in a phage capsid

Cecilia Bores and B. Montgomery Pettitt

Phys. Rev. E **101**, 012406 — Published 13 January 2020

DOI: 10.1103/PhysRevE.101.012406

Structure and the Role of Filling Rate on Model dsDNA Packed in a Phage Capsid

Cecilia Bores and B. Montgomery Pettitt

University of Texas Medical Branch,

Department of Biochemistry and Molecular Biology

(Dated: November 8, 2019)

Abstract

The conformation of DNA inside bacteriophages is of paramount importance for understanding packaging and ejection mechanisms. Models describing the structure of the confined macromolecule have depicted highly ordered conformations, such as spooled or toroidal arrangements that focus on reproducing experimental results obtained by averaging over thousand of configurations. However, it has been seen that more disordered states, including DNA kinking and the presence of domains with different DNA orientation can also accurately reproduce many of the structural experiments. In this work we have compared the results obtained through different simulated filling rates. We find a rate dependence for the resulting constrained states showing different anisotropic configurations. We present a quantitative analysis of the density distribution and the DNA orientation across the capsid showing excellent agreement with structural experiments. Second, we have analyzed the correlations within the capsid finding evidence of the presence of domains characterized by aligned segments of DNA characterized by the structure factor. Finally, we have measured the number and distribution of DNA defects such as the emergence of bubbles and kinks as function of the filling rate. We find the slower the rate the fewer kink defects that appear and they would be unlikely at experimental filling rates with our model parameters. DNA domains of various orientation get larger with slower rates.

I. INTRODUCTION

Bacteriophages are genome-delivery machines that infect bacterial cells. The importance of these viruses lies in their ability to kill pathogenic bacteria [1] and their key role in the emergence of both molecular and physical biology [2–4]. In this work, we consider a coarse grained model with the packing density of bacteriophage ϕ29[5], whose relatively short genome makes it an ideal candidate for computational simulations. This system contains a double-stranded DNA (dsDNA) molecule of 19285 bp genome confined inside its capsid. The genome packaging to near liquid-crystalline density is done in the biological setting by an ATP powered portal motor, able to overcome forces up to 60pN [6, 7]. DNA packaging is a critical aspect of dsDNA bacteriophages life-cycle and during this process defects such as knots, kinks, loops, etc may emerge that hinder both the insertion and the ejection processes of the DNA. Probing the conformation of the DNA molecule inside phages is very

challenging for experiments, mainly because in most cases they only provide information about the probability distribution of DNA density by averaging data from a large number of phages. Simulations are a tool that can model the ensembles of structures and the process of DNA packaging thus producing a probability distribution of structure of the DNA.

Many studies have been performed to better understand how DNA packs inside the capsid of bacteriophages [5, 8, 9], but aspects of the problem are not resolved. In order to deal with typical genome sizes in phages, computational studies have used either continuum-elastic theories [10–13] or coarse-grained models for computer simulations [14–19]. Both approaches consider DNA essentially as an elastic rod modeling B-form dsDNA with a persistence length of ∼50 nm; they predict a highly ordered spool-like conformation that can vary depending on capsid characteristics and method of filling [9]. Whereas these studies are in agreement with the ring-like density maps found by cryo-electron microscopy experiments and three-dimensional image reconstruction [20–23], the ejection times predicted are several orders of magnitude larger than those seen experimentally [24]. In addition, as it was noted in Ref. [25], these image reconstructions only show averaged structures obscuring some details of the DNA domains inside phage capsids. These domains were revealed early on by cryo electron microscopy and X-ray [26–28] and more recent studies of DNA in vitro [29, 30] and are incompatible with the near-perfect spool models. A recent simulation considering the presence of kinked DNA conformations has shown that very disordered and improbable conformations are also able to reproduce the experimental ring-like distribution, while reducing the electrostatic component of the energy and pressure of the confined genome [31]. Even a set of unconnected DNA segments confined in a sphere lead to density profiles showing ring-like behavior as a result of surface-induced ordering [32]. Given the lack of polymer correlations, that work set an unrealistic upper bound on the amount of DNA disorder possible while demonstrating the simple requirement for correlations to agree with averaged experiments. Here we consider what kinds and how much order/disorder is reasonable (or required) when a DNA is confined in the phage capsid using a fully polymeric model with sequence dependent properties.

It is known that the molecular motor responsible for DNA insertion into the phage capsid must overcome electrostatic repulsions, volume exclusion and DNA flexibility. For this reason, in order to analyze the degree of order/disorder of the confined DNA it will be essential to take into account as many features of the polymer as possible. Here we have

employed a single-nucleotide level coarse-grained model of DNA [33], to mimic the packaging process using simulations. To simplify and avoid confounding issues with the details of the protein capsid we have used a simplified model for the elongated capsid of the phage: a purely repulsive spherical wall. This simple model is able to capture the spatial confinement of the DNA and the high density of the final state in a computationally efficient way. By considering an ensemble of statistically independent simulations we have found that, although the individual structures diverge due to the nonlinear dynamics, certain common features can be extracted showing evidence of both order and disorder present in the DNA final conformation. Finally, we note here that the actual filling rate induced by the portal motor, 100 bp/s [7], is impossible to achieve computationally currently with the level of detail used here; so the process needs to be accelerated. We use different filling rates to determine the sensitivity of the properties to rate. The confined DNA molecule has been shown to exhibit non-equilibrium dynamics due to kinetic constrains on packaging timescale [34] - we have found that a rate slow enough to allow DNA diffusion inside the capsid strongly impacts the DNA final conformation, individually and on average.

II. METHODS

DNA packaging process was modeled by performing molecular dynamics simulations. We used the freely available oxDNA2 package taking advantage of its CUDA acceleration [35]. Simulations were performed at a fixed temperature of 300.15K (27C) by using a thermostat emulating Brownian dynamics - the so-called "John" thermostat in oxDNA package - with a time step of 3.03 fs. DNA was represented using oxDNA2, a nucleotide-level coarse-grained potential model using rigid nucleotides that account for the sugar-backbone connectivity, excluded volume, the hydrogen bonding and stacking between the bases, which has shown to successfully reproduce many thermodynamic, structural and mechanical properties of DNA [36–38]. This model has been parameterized to fit experimental melting temperatures, persistence lengths and successfully reproduces the effect of salt and groove asymmetry on DNA elasticity [36, 37]. A Debye-Hückel screening term incorporated into oxDNA[38] is used to account for the effect of monovalent salt on DNA electrostatics. The ionic strength was set at 1 M, a value that is not meant to model the cytosol but to reflect the concentrated state in the final packed capsid. Solvent is considered implicitly in the effective potential.

While this simplistic representation of the electrostatic interactions allows one to perform molecular dynamics simulations with the large number of nucleotides considered here, it may also compromise some resulting local structure between strands caused by the presence of bridging water molecules or/and ions in concentrated DNA.

We have used a simplified model to represent the confining nature of the mature prolate capsid of phage ϕ29 consisting of a spherical, rigid and purely repulsive harmonic wall characterized by the half harmonic potential $E_{capsid} = k(r - R)^2$ for $r > R$, where R is the radius of the capsid, r is the distance of the nucleotide to the center of the capsid, and $k = \epsilon/\sigma^2$ with ϵ=4.142$\times 10^{-20}$J and σ=8.518$\times 10^{-10}$m. The radius of the capsid, 21.5 nm, was chosen to reproduce the estimated value of DNA density or concentration inside the phage (around 0.5 g/ml [5]), given that a 10 bp long dsDNA segment weights 6500 g/mol. Pairs of nucleotides were inserted two at a time into the capsid by placing them at the opening of the mouth applying harmonic forces to both base and phosphate groups. The intensity of these forces, 12.1575 nN, ensures an average displacement along the mouth during the simulation, but do not exclude highly energetic configurations. To avoid excessive overlap of the new nucleotides being inserted with those already present in the capsid we have built a "entry portal" consisting of a cylinder attached to the spherical capsid of radius 2.1 nm that decreases to 1.3 nm at 4.50 nm from the capsid. We have considered two filling rates to introduce the DNA molecule inside the capsid: 3.03 10^{10} bp/s (*fast rate*) and a rate of 3.03 10^{9} bp/s (*slow rate*). All the structural features shown in this article have been performed considering the center of mass of each nucleotide, and correspond to the average over a number of independent runs: 15 and 33 for the slow and fast rates respectively.

The distribution and orientation of the DNA molecule within the capsid have been quantitatively assessed by means of density and angular correlations. First, the radial density profile has been used to describe the probability of finding DNA at a given distance from the capsid wall. Second, we have quantified DNA orientation by looking at the angles between the vectors $\mathbf{r}_{DNA}$ (vector tangential to the DNA molecule at each pair-base) and $\mathbf{r}_{radial}$ (radial vector in spherical coordinates) or $\mathbf{r}_{cylindrical}$ (vector tangential to the cylinder defined by the portal axis). These angles consider respectively about whether the DNA polymer shows a spherically or coaxially spooled preferential conformation. Being aware of the possible different behavior depending on the distance to the capsid wall, we have considered separately the DNA located in each of three distinct layers that can be distinguished in

the radial density profile and in the inner region of the capsid. We have calculated the histograms of the cosines and weighted them with the number of base-pairs present in each of the regions to being able to compare the results.

Pair correlation functions provide additional information about the degree of order in the system and we have used them to detect and quantify the presence of ordered domains of DNA inside the capsid. We have calculated the pair correlation function $g(r)$, giving the probability of finding a base-pair at a distance r from another one, and the angular correlation function $G_2(r)$ that measures the relative orientation of two DNA segments separated a distance r. $G_2(r)$ is defined as $G_2(r) = 5 < P_2(cos\theta_{12}) >_r$ where $< ... >_r$ denotes the time and ensemble average in a spherical shell. $P_2(x) = (3x^2 - 1)/2$ is the Legendre polynomial of order 2, and θ_{12} is the angle between the axes of two DNA segments [39].

To further characterize the presence of ordered domains we have calculated the structure factor defined as the Fourier transform of the pair density distribution function:

$$S(k) = 1 + \rho \int exp(-ikr)g(r)dr$$

where ρ is the microscopic density and k is the scattering vector. The structure factor reflects the internal configuration of the B form of DNA through several maxima at wide scattering angles, the presence of the capsid via a short-wavelength modulation with a reciprocal spacing compatible with the capsid internal diameter, and DNA packing in parallel arrays whose distance is given by the position of a strong peak at intermediate angles, absent for empty phages [40]. The width of this peak allows the estimation of the apparent size of the domains exhibiting a regular orientation, D, by applying the Scherrer equation [41], $D \approx \pi/d$, where d is the width at half peak-height.

The potential for spontaneous defect formation in the confined DNA molecule shifting it away from the perfect B form has been explored. We have defined kinks as the base pairs characterized by a large roll angle (larger than 1.1 rad as in Ref. [42]) between two continuous DNA segments consisting of 6 base pairs, and bubbles as the base pairs with a distance between the bases larger than 1.5 times the average equilibrium distance between them (0.34 nm).

III. RESULTS

A. DNA final conformation

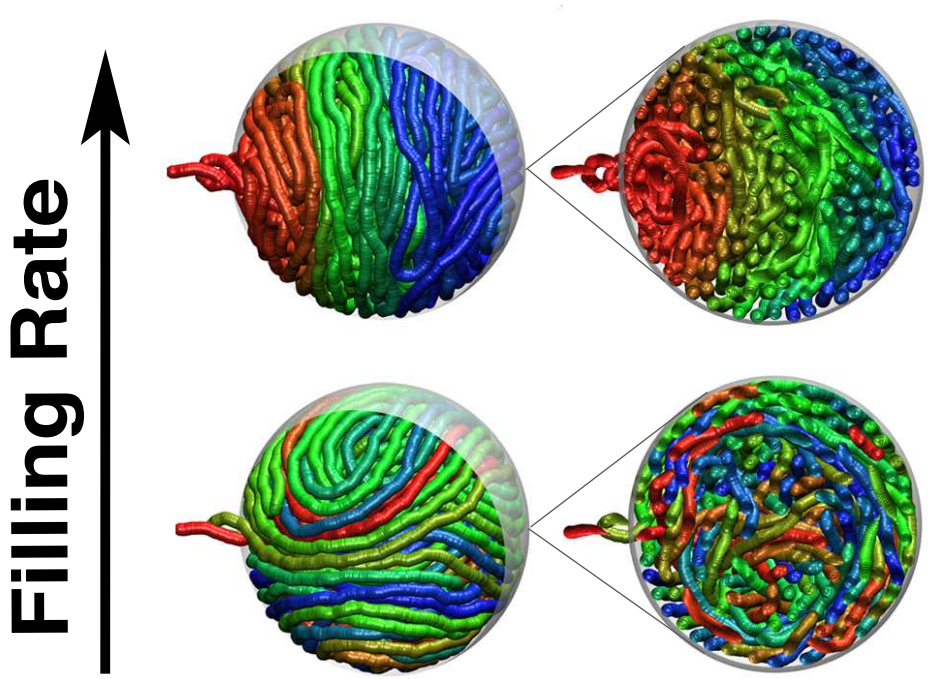

FIG. 1. Typical configurations resulting from a MD simulation of DNA filling inside phage ϕ29 capsid. Upper row corresponds to the fast rate of 3.03 10^{10} bp/s and bottom row to the slow rate of 3.03 10^{9} bp/s. Sections parallel to the mouth axis are also provided (right column). We note here that only the center of mass of each base-pair has been represented for clarity. Color indicates the first (blue) and last (red) parts of the inserted genome.

We performed MD simulations modeling the DNA packaging process inside the capsid as described above. We found that each of these simulations yields a different final conformation, but certain average features emmerge, as we will show below. In Fig. 1 we display typical conformations resulting from our MD simulations where the coloring scheme allows

one to distinguish between the first part or head (blue) and the last part or tail (red) of the inserted genome. The upper row corresponds to the fast filling rate and the lower row to a rate ten times slower. A view of the system following the mouth axis and a cross section showing DNA structure inside the capsid (right column) are shown. In all these representations and the analysis done below, only the center of mass of each base-pair has been considered.

Clearly different DNA conformations arise depending on the filling rate. The final structure of the confined DNA for the slowest rate exhibits more homogeneous features than for the fastest rate we have considered that shows an anisotropic preferential arrangement perpendicular to the filling axis. We can also see that the first inserted nucleotides for the fast rate go to the far side and layer showing that diffusion and mixing inside the capsid has been highly constrained. To better illustrate this feature, Figure S1 in Supplemental Material [43] shows snapshots at different stages of the filling process for both filling rates. The filling rate we have called fast does not allow the mixing diffusion of the genome throughout the capsid volume while being inserted, and this is especially clear for the early stages of the filling process (panels a and b). This is also reflected in the density profile of Figure S2 in Supplemental Material [43], where we have divided the capsid volume into three spherical sectors along the filling axis: close to the portal, equatorial and far from the portal. While DNA density is more isotropic and mixed for the slow rate and similar in both sectors, it tends to stay closer to the mouth for the fast rate.

We wish to understand the features of the confined DNA molecules and how they differ depending on the filling rate. The radial density profile of the confined DNA averaged over all the independent simulations is plotted in Figure 2 for the two filling rates considered. The shape suggests a layered structure near the capsid wall with 3 to 4 pronounced peaks separated by a distance around 2.44 nm in excellent agreement with the experimental value [22]. The density in the central shell, excluding the 3 outer layers, is around 0.42 base pairs/nm^3 (0.45 g/ml). We note that the error is much higher at small values of $r - r_0$ due to poorer statistics in the center of the sphere where the volume in the sampled shells is smaller.

The radial density profile corresponding for the total DNA molecule is very similar for both filling rates considered here, but there is a greater difference when analyzing separately the first, intermediate and final segments. This analysis is shown in Figure S3 of Supple-

mental Material [43] and quantitatively reflects that the first inserted DNA is confined in the outer layers leading to an inhomogeneous DNA distribution for the fastest rate versus a more homogenous repartition for the slowest rate. The latter showing almost no difference between the initial, intermediate and final sections of the genome inserted. Finally, the evolution of the radial density profile during the filling process for both filling rates is shown in Figure S4 of Supplemental Material [43] which shows that DNA is evenly distributed across the capsid from the beginning and that the peaks near the wall arise progressively as the DNA density increases. Those peaks clearly reflect the density waves or correlations with the capsid wall one would expect in any liquid system of sufficient density [31].

DNA shows a clear trend to arrange in a coaxial spooled conformation when we fill the capsid at the fastest pace, especially for the outermost layer, but this tendency almost vanishes for the slowest rate. This feature is visible from the snapshots in Figure 1 but it has also been quantitatively analyzed looking at the distribution of the cosine of the angle $\alpha_{cylindrical}=\alpha(\mathbf{r}_{DNA},\ \mathbf{r}_{cylindrical})$ between DNA segments and the vector tangential to the cylinder defined by the portal axis, which is plotted in Figure S5 in Supplemental Material [43]. Here 1 means DNA is cylindrically spooled around the axis of the portal. In contrast,

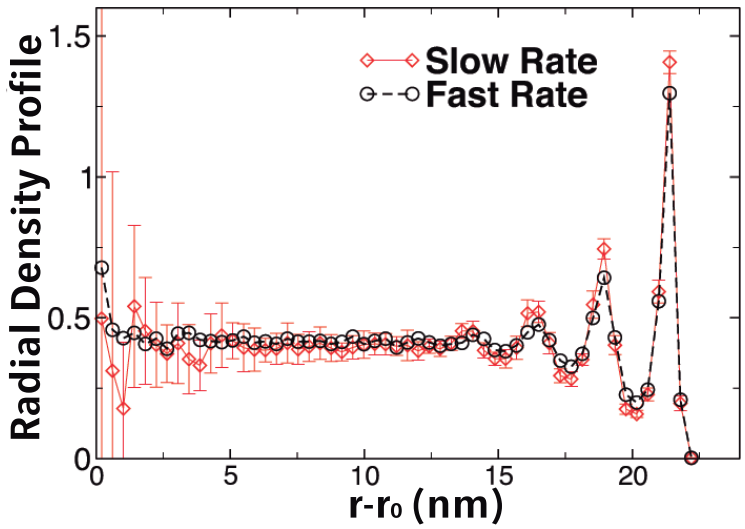

FIG. 2. Spherical density profiles for the DNA molecule packaged in a spherical model of phage ϕ29 through the fast (black dashed line) and slow (red solid line) filling rates where $r - r_0$ is the distance to the center of the spherical capsid. Error bars for the fast rate are similar to those of the slow rate and they are not plotted for clarity.

the angle α_{radial}=$\alpha(\mathbf{r}_{DNA}, \mathbf{r}_{radial})$ gives information about the angle between DNA segments and the radial vector perpendicular to the capsid wall at each point, see Figure S6 in the Supplemental Material [43]. In this case 0 corresponds to DNA parallel to the capsid wall and 1 perpendicular. There were no significant differences found in $\cos(\alpha_{radial})$ with respect to filling rate. The first layer in both cases showed at least twice the population parallel to the wall ($cos = 0$).

B. Signatures of order and disorder

We can see from the density correlation function (left in Figure 3) that besides the strong local correlations between consecutive nucleotides, separated by 0.34 nm, there is also intermediate range order reflected by the peak at 2.8 nm, near the average distance between neighbor DNA segments; however there is no dependence of this property on filling rate. On the other hand, the angular correlation function plotted in right graph of Figure 3 shows that the orientation between DNA segments shows some difference with respect to filling rate. The former suggests the existence of domains where neighboring segments of DNA arrange parallel to each other, which is in agreement with experimental results from cryo electron microscopy [29, 44] and can also be noticed from the snapshots plotted in Figure 1.

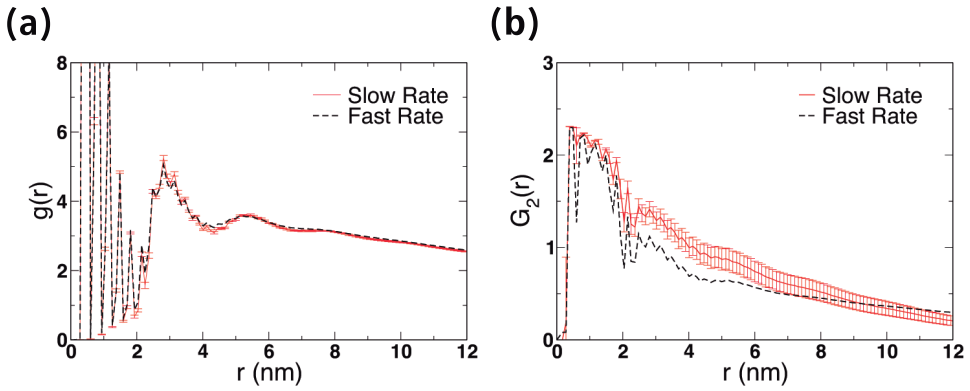

FIG. 3. Density (a) and Angular (b) correlation functions for fast (dashed black) and slow (solid red) filling rates. Error bars for the fast rate are similar to those of the slow rate and they are not plotted for clarity.

Small-angle X-ray scattering has been used to characterize DNA conformation inside phages in experiments [26, 45, 46] predicting the presence of domains of hexagonally packaged DNA. We have calculated the structure factor of the confined genome for both filling rates, Fig. 4. It shows the signature of long-range order through a rippled modulation at q =0.153 nm^{-1}, corresponding to the capsid size in the direct space: $2\pi/q = 43$ nm. The intermediate-range order is reflected in the peak around q_{max}=2.59 nm^{-1} and, assuming hexagonal order, yields an estimate of the inter-helix DNA distance as $4\pi/\sqrt{3}q_{max} = 2.80$ nm. To better compare with hexagonal order we have also shown in Figure 4 (dotted line) the structure factor corresponding to a 3x3 array of parallel DNA segments 50 pair-bases long. This value agrees with previous experiments [5, 46] and with the position of the first peak in $g(r)$ (Figure 3). We have found that the apparent size of the domains exhibiting a regular orientation is, according to the Scherrer equation [41], $D \approx 5.68$ nm for the fast rate and somewhat larger $D \approx 7.30$ nm for the slow rate, which agrees with the angular correlation in Fig. 3. This suggests a larger angular correlation for the slower rate. Figure S7 in Supplemental Material [43] shows the evolution of the structure factor during the filling process for both packing rates, indicating that the DNA segments come closer and the domains of aligned DNA become bigger as the density inside the capsid increases.

The experimental detection of DNA defects inside the bacteriophages is very challenging and, to our knowledge, has not been well explored. However, the presence of high-affinity ethidium-binding sites found in T7 has been interpreted as an experimental evidence of kinked DNA sites within the capsid [47]. This feature could be important since kinks have been seen to reduce the repulsive electrostatic component of the free energy and pressure of the confined genome [31]. We have analyzed the structure of the DNA molecule inside the virus during the filling process and find that some defects such as kinks and bubbles arise spontaneously. The spatial distribution and number of defects have been analyzed, see Figures 5 and 6 respectively, and they strongly depend on the filling rate. We have found that around 80% of the defects emerge close to the portal when DNA is packed using the fastest rate, but the distribution is more homogenous and far less numerous when using the slowest rate. The distribution within the capsid layers however is relatively uniform in both cases. The number of large roll angles is bigger for the fast rate suggesting that most of this defects are due to the inability of DNA to "relax" while being packed. Furthermore, we have explored the effect of temperature and ionic strength finding that higher temperatures and

lower salt concentration may increase the number of defects in the DNA slightly. Higher temperature and lower salt concentration do not seem to modify any other feature of the DNA conformation analyzed here (data not shown).

It has been seen that certain DNA sequences have higher probability to break or kink than others due to a different DNA stability [42, 48]. However, even though the model we are using includes a sequence-dependent parametrization of the hydrogen-bonding and stacking interactions, we have found that defects emerge for this model with little sequence dependence for the statistics at hand. We note here that the time scale of our simulations is very short (by many orders of magnitude) compared to the actual packing rate, the number of independent configurations we are averaging over is small and we are not twisting the DNA.

IV. DISCUSSION AND CONCLUSION

In this contribution we have presented a systematic and quantitative study to consider the effect of filling the capsid of

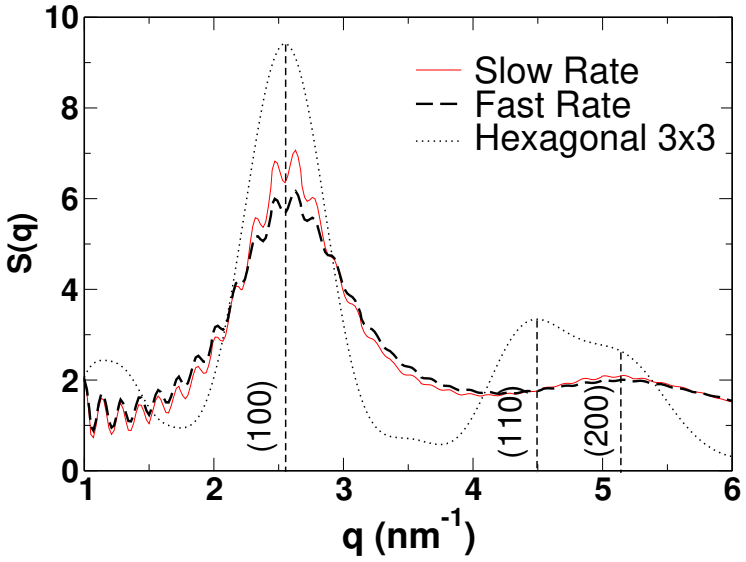

FIG. 4. Structure factor for the last conformation of the DNA molecule averaged over all statistically independent simulations. Dotted line shows the structure factor corresponding to a 3x3 hexagonal array of parallel chains of spheres separated by 0.34 nm (same as the nucleotides in our model).

phage ϕ29. The DNA distribution inside the capsid, the intermediate-range ordered domains and the emergence of defects evolve during the filling process have been considered. We showed that many structural features of the confined DNA molecule found experimentally can be reproduced by using a coarse grained model for the DNA and a simple repulsive spherical wall for the capsid of the ϕ29 phage. Our simulations have predicted the presence of DNA layers in the outermost region, with the distance between these layers similar to that found experimentally, 2.44 nm [22]. The angular correlation function and the structure factor have revealed the presence of domains of aligned DNA segments in agreement with cryoEM and Xray experiments [5, 26, 29, 44, 46]. The distance between neighbor DNA segments is of 2.85 nm, justifying the general assumption of some local hexagonal packing order inside the phage.

On the other hand, we have found that too fast a filling rate arrests DNA diffusional mixing within the capsid and yields an inhomogenous DNA distribution and coaxial orientation. Using this fast filling rate causes the emergence of more kinks in the DNA molecule than a slower rate, especially at the end of the process. If we linearly extrapolate the number of

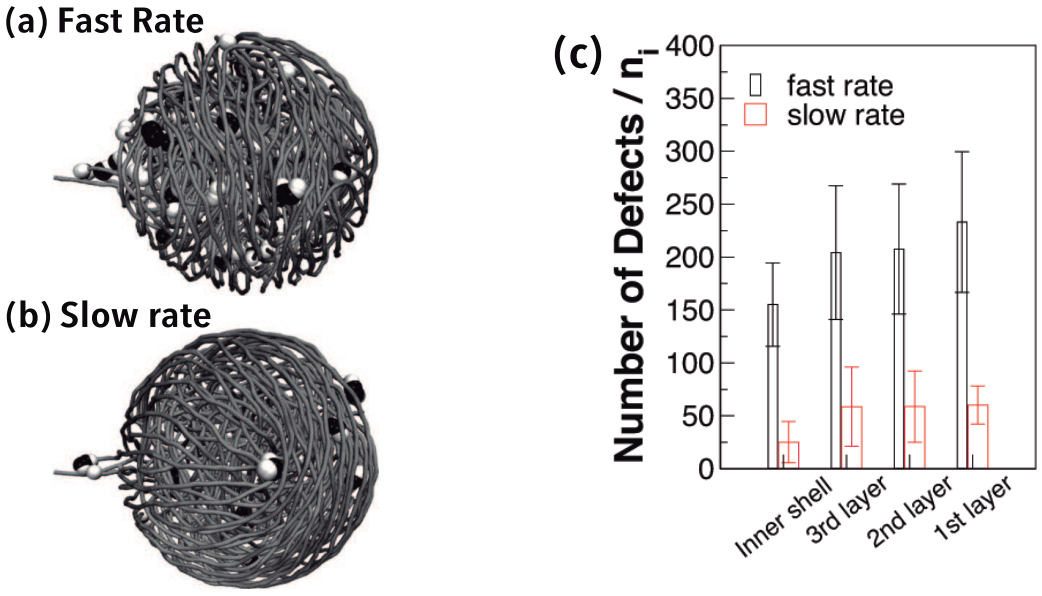

FIG. 5. Snapshots of the final conformation of DNA confined inside the capsid for the fast (a) and slow (b) rates emphasizing the presence of defects: black corresponds to bubbles and white to kinks. (c) Histograms of the distribution of kinks among the layers defined by the density profiles. The number of defects has been normalized by the fraction of base-pairs contained within each layer (n_i= number of base-pairs in shell i / total number of base-pairs)

defects expected to the experimental filling rate we would rarely expect to see such a defect under the idealized conditions of the model considered here. Nevertheless, more realistic features such as capsid shape and size, presence of multivalent ions, burst and dwell stages or twisting forces while filling may change the probability. Finally, the size of the domains of hexagonally packed DNA segments is also affected by the filling rate, being larger for the slowest rate considered here. Our computational limit for the filling rate leads to a simulation time in the microsecond range, comparable to previous simulations such as the ones in Ref. 49, 50 and 15 which is over a million times faster than the real process. This comparison is not straightforward though because we are considering a constant rate with no dwells. We suspect that using a different filling approach considering a variable filling rate or including pauses especially at the final packaging stage may affect the results and

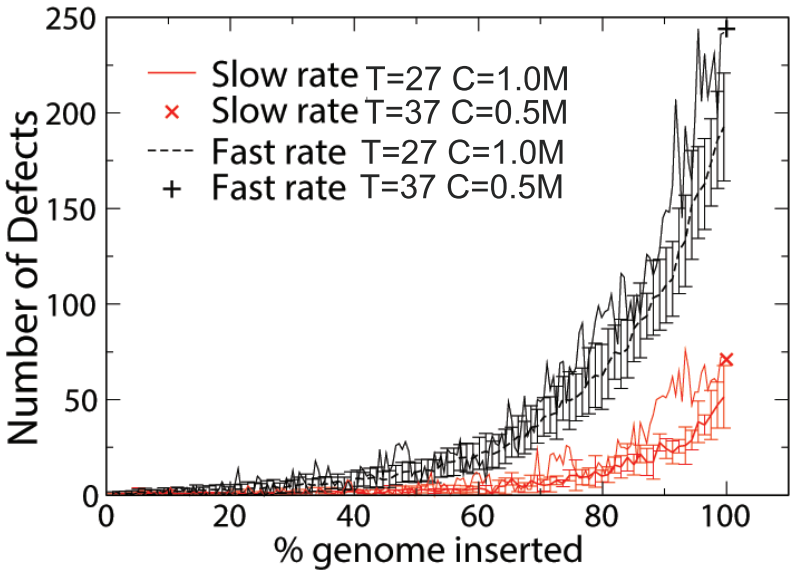

FIG. 6. Evolution of the emergence of large roll angles in the DNA molecule during the filling process for both fast and slow rates averaged over all the independent simulations for each case. The effect of a bigger temperature and a lower salt concentration are represented by lines ending in a symbol corresponding to a single simulation with a temperature of 37C and salt concentration equal to 0.5M. The other data showing the error bars correspond to the standard ensemble ofsimulations performed in this work at a temperature of 27C and a salt concentration of 1M.

we intend to analyze this feature in future contributions.

Ion concentration affects the DNA persistence length [51] and the model we are using is able to capture this behaviour [36]. Preliminary simulations show that, for the fastest rate considered here, there is no significant difference in the final DNA structure for different concentrations of monovalent salts. However, it has been seen experimentally that the presence of multivalent ions affect both DNA packaging and portal motor function in phages [52].

Our present study used a simple spherical containment model for the capsid. Even with such a simplification we found two dominant modes of filling structures result: One with the DNA coiling around the filling axis and one with structures and domains predominantly perpendicular to the first. Many features in a more realistic capsid model might contribute to the emergence of these or other patterns. Specific molecular recognition between the capsid proteins and the DNA could cause profound ordering and seems evident in some recent virus structures [53]. In future works more realistic models for the capsid - such as an elongated shape or the presence of attractive/repulsive sites - and for the filling process - torsional forces twisting the DNA or capsid expansion and contraction - may also contribute to modulate the effect of each studied feature of the confined DNA.

ACKNOWLEDGMENTS

The authors thank Dr Marc Morais for interesting conversations. We gratefully acknowledge the Robert A. Welch Foundation (H-0037 at the start and H-0013 at the end) and the National Institutes of Health (GM-066813) for partial support of this work. This work used the Extreme Science and Engineering Discovery Environment (XSEDE), which is supported by National Science Foundation grant number ACI-1548562.

---

[1] E. C. Keen, Front Microbiol **3**, 238 (2012).

[2] A. D. Hershey and M. Chase, J Gen Physiol **36**, 39 (1952).

[3] G. P. Smith, Curr. Opin. Biotechnol. **2**, 668 (1991).

[4] C. E. Catalano, D. Cue, and M. Feiss, Mol. Microbiol. **16**, 1075 (1995).

[5] W. C. Earnshaw and S. R. Casjens, Cell **21**, 319 (1980).

[6] N. Keller, Z. T. Berndsen, P. J. Jardine, and D. E. Smith, Phys Rev E **95**, 052408 (2017).

[7] D. E. Smith, S. J. Tans, S. B. Smith, S. Grimes, D. L. Anderson, and C. Bustamante, Nature **413**, 748 (2001).

[8] A. S. Petrov and S. C. Harvey, Biophysical Journal **95**, 497 (2008).

[9] L. W. Black and J. A. Thomas, Condensed genome structure, in *Viral Molecular Machines*, edited by M. G. Rossmann and V. B. Rao (Springer US, 2012) pp. 469–487.

[10] S. Tzlil, J. T. Kindt, W. M. Gelbart, and A. Ben-Shaul, Biophys J **84**, 1616 (2003).

[11] P. K. Purohit, M. M. Inamdar, P. D. Grayson, T. M. Squires, J. Kondev, and R. Phillips, Biophys J **88**, 851 (2005).

[12] P. K. Purohit, J. Kondev, and R. Phillips, Proc Natl Acad Sci U S A **100**, 3173 (2003).

[13] J. Kindt, S. Tzlil, A. Ben-Shaul, and W. M. Gelbart, Proc Natl Acad Sci U S A **98**, 13671 (2001).

[14] J. Arsuaga, R. K. Z. Tan, M. Vazquez, D. W. Sumners, and S. C. Harvey, Biophysical Chemistry **101-102**, 475 (2002).

[15] J. C. LaMarque, L. Le Thuc-vy, and S. C. Harvey, Biopolymers **73**, 348 (2003).

[16] I. Ali, D. Marenduzzo, and J. M. Yeomans, Phys Rev Letters **96**, 208102 (2006).

[17] A. J. Spakowitz and Z.-G. Wang, Biophysical Journal **88**, 3912 (2005).

[18] C. Forrey and M. Muthukumar, Biophys J **91**, 25 (2006).

[19] A. S. Petrov and S. C. Harvey, J Struct Biol **174**, 137 (2011).

[20] Y. Tao, N. H. Olson, W. Xu, D. L. Anderson, M. G. Rossmann, and T. S. Baker, Cell **95**, 431 (1998).

[21] J. Tang, N. Olson, P. J. Jardine, S. Grimes, D. L. Anderson, and T. S. Baker, Structure **16**, 935 (2008).

[22] L. R. Comolli, A. J. Spakowitz, C. E. Siegerist, P. J. Jardine, S. Grimes, D. L. Anderson, C. Bustamante, and K. H. Downing, Virology **371**, 267 (2008).

[23] M. M. Farley, J. Tu, D. B. Kearns, I. J. Molineux, and J. Liu, Journal of Structural Biology **197**, 163 (2017).

[24] A. S. Petrov, S. S. Douglas, and S. C. Harvey, J Phys Condens Matter **25**, 115101 (2013).

[25] S. R. Casjens and I. J. Molineux, Short noncontractile tail machines: Adsorption and dna delivery by podoviruses, in *Viral Molecular Machines*, edited by M. G. Rossmann and V. B. Rao (Springer US, 2012) pp. 143–179.

[26] A. C. North and A. Rich, Nature **191**, 1242 (1961).

[27] M. Gellert and D. R. Davies, J Mol Biol **8**, 341 (1964).

[28] J. Lepault, J. Dubochet, W. Baschong, and E. Kellenberger, EMBO J **6**, 1507 (1987).

[29] A. Leforestier and F. Livolant, Journal of Molecular Biology **396**, 384 (2010).

[30] M. Frutos, A. Leforestier, J. Degrouard, N. Zambrano, F. Wien, P. Boulanger, S. Brasiles, M. Renouard, D. Durand, and F. Livolant, J Phys Chem B **120**, 5975 (2016).

[31] C. G. Myers and B. M. Pettitt, Journal of Computational Chemistry **38**, 1191 (2017).

[32] C. G. Myers and B. M. Pettitt, J Chem Phys **138**, 071103 (2013).

[33] T. E. Ouldridge, A. A. Louis, and J. P. Doye, J Chem Phys **134**, 085101 (2011).

[34] Z. T. Berndsen, N. Keller, S. Grimes, P. J. Jardine, and D. E. Smith, Proc Natl Acad Sci U S A **111**, 8345 (2014).

[35] L. Rovigatti, P. ulc, I. Z. Reguly, and F. Romano, Journal of Computational Chemistry **36**, 1 (2015).

[36] B. E. K. Snodin, F. Randisi, M. Mosayebi, P. Sulc, F. Romano, T. E. Ouldridge, R. Tsukanov, E. Nir, A. A. Louis, and J. P. K. Doye, Journal of Chemical Physics **142**, 234901 (2015).

[37] E. Skoruppa, M. Laleman, S. K. Nomidis, and E. Carlon, The Journal of Chemical Physics **146**, 214902 (2017).

[38] Q. Wang and B. M. Pettitt, Biophysical Journal **106**, 1182 (2014).

[39] E. Lomba, C. Martin, N. G. Almarza, and F. Lado, Phys Rev E **71**, 046132 (2005).

[40] W. Earnshaw, S. Casjens, and S. C. Harrison, J Mol Biol **104**, 387 (1976).

[41] A. Guinier, *X-ray Diffraction. In Crystals, Imperfect Crystals, and Amorphous Bodies* (W. H. Freeman and Company, 1963).

[42] J. SantaLucia, J., H. T. Allawi, and P. A. Seneviratne, Biochemistry **35**, 3555 (1996).

[43] See Supplemental Material at [URL will be inserted by publisher] for snapshots, radial density profiles and correlation functions of the confined DNA at different stages of the packaging process, as well as orientational distribution profiles of the DNA.

[44] M. De Frutos, A. A. Leforestier, and F. F. Livolant, Biophysical Reviews and Letters **09**, 81 (2014).

[45] W. C. Earnshaw and S. C. Harrison, Nature **268**, 598 (1977).

[46] J. A. Subirana, J. Lloveras, M. Lombardero, and E. Viuela, Journal of Molecular Biology **128**, 101 (1979).

[47] G. A. Griess, P. Serwer, and P. M. Horowitz, Biopolymers **24**, 1635 (1985).

[48] Q. Wang, C. G. Myers, and B. M. Pettitt, J Phys Chem B **119**, 4937 (2015).

[49] A. S. Petrov and S. C. Harvey, Structure **15**, 21 (2007).

[50] A. Cordoba, D. M. Hinckley, J. Lequieu, and J. J. de Pablo, Biophys J **112**, 1302 (2017).

[51] Z. Margarita, A. Potyahaylo, and D. Hovorun, Biopolymers and Cell **33**, 81 (2017).

[52] D. N. Fuller, J. P. Rickgauer, P. J. Jardine, S. Grimes, D. L. Anderson, and D. E. Smith, Proceedings of the National Academy of Sciences **104**, 11245 (2007).

[53] X. Dai, Z. Li, M. Lai, S. Shu, Y. Du, Z. H. Zhou, and R. Sun, Nature **541**, 112 (2017).